Finite-cluster multiple-scattering theory of x-ray bremsstrahlung isochromat spectra

O. Šipr, J. Vackář, and A. Šimůnek
Institute of Physics, Czechoslovakian Academy of Science, Cukrovarnická 10, 162 00 Praha 6, Czechoslovakia
(Received 13 November 1990)

A real-space finite-cluster multiple-scattering method for the calculation of x-ray bremsstrahlung isochromat spectra is presented. This method makes it possible to calculate the spectra in both the near and the extended energy region even for materials lacking full translational symmetry. Various approximations can be introduced within the multiple-scattering formalism very naturally so that an optimal ratio between the computational effort and the accuracy can be achieved. We illustrate the efficiency of this method by calculating the isochromat spectra of Cu and Pd and comparing them with experiment. Both the dipole and the quadrupole contributions to the bremsstrahlung transition-matrix elements are quantified and the latter are found to be negligible. The choice of the most suitable one-electron potential is discussed. The spectra calculated by using a non-self-consistent Mattheiss potential are very close to the results obtained using a self-consistent potential. The energy-dependent Dirac-Hara exchange term gives better results than the energy-independent Kohn-Sham exchange potential.

I. INTRODUCTION

X-ray bremsstrahlung isochromat spectroscopy (XBIS) has attracted a considerable interest in recent years. This interest was caused partly by the effort to understand the physical nature of the XBIS process (importance of XBIS matrix elements,[1-3] validity of the one-electron description,[1,4,5] etc.), partly by the endeavor to clarify its relation to x-ray-absorption spectroscopy (XAS).[4,6-9]

XBIS is predominantly used in two energy regions: (i) in the near energy region up to ~40 eV above the Fermi level E_F, and (ii) in the extended energy region ~100–500 eV above E_F. In the near energy region XBIS has become a valuable tool for investigating the unoccupied electron states, and in many respects is analogous to XANES (x-ray-absorption near-edge structure). In the extended energy region XBIS reflects mainly the structural properties of the investigated material, and is analogous to EXAFS (extended x-ray-absorption fine structure).

It was shown that one-electron theory describes the XBIS spectra satisfactorily.[1,10,9] The relevant quantities related to the electronic structure (e.g., the density of states or the scattering matrix) can be calculated either taking the whole infinite crystal into account, or limiting one's attention only to a finite cluster of atoms. The latter approach, though formally not as accurate as the former, can be of great importance in studying XBIS of noncrystalline materials and/or in an extended energy range.

The aim of this paper is to present the finite-cluster multiple-scattering (FC-MS) theory of XBIS and to discuss its various aspects. We draw an intuitive picture of the XBIS process, trying to pick out the main physical ideas which form the "inner philosophy" of the FC-MS approach to XBIS. The detailed derivation of final equations, which can be used for calculating XBIS spectra, is presented. Since the validity of the dipole approximation in XBIS was questioned,[11] we quantify the dipole and the quadrupole contributions to the XBIS matrix elements, finding that the quadrupole term is negligible. We show that making use of a non-self-consistent Mattheiss potential[12,13] results in XBIS spectra which are very similar to those obtained using a self-consistent potential. We tested two choices of exchange potential, namely the widely used Kohn-Sham potential[14] and the energy-dependent Dirac-Hara potential,[15] over a broad energy range, and found that making use of the Dirac-Hara potential affects the peak positions in the extended part of the spectrum significantly.

II. BASIC THEORY OF XBIS

A. Intuitive picture

Bremsstrahlung isochromat spectroscopy is based on the following process: A sample made of investigated material is subjected to a bombardment by electrons of known energy E_i. These electrons are decelerated inside the sample and the bremsstrahlung radiation ("continuous spectrum") arises.

The energy of the initial electron state E_i, the energy of a particular final electron state E_f, and the energy of the bremsstrahlung radiation emitted during this particular transition $\hbar\omega$ are bound by a simple relation

$$\hbar\omega = E_i - E_f \ . \tag{1}$$

In order to map the density of unoccupied states of energy E_f, the initial electron energy E_i is varied while the intensity of the bremsstrahlung radiation of fixed energy $\hbar\omega$ (so-called *isochromat energy*) is measured.

It is convenient to choose the experimental conditions so that the energy of the registered radiation $\hbar\omega$ would be large in comparison with the energy of final electrons, i.e.,

$$E_i - E_f \gg E_f - E_F \ , \tag{2}$$

where E_F is the Fermi energy. It is obvious that such a great deceleration of the initial electron must be caused by an enormous electrostatic field, which occurs only near the atomic core. Hence, the final-state electron begins its path throughout the crystal in this region. As a result of this, unoccupied electron states "as seen from the core region" of a particular atom (referred to as the *central* atom in the following text) are investigated in XBIS.[1,9]

The probability $w(E_i)$ of a radiative transition of the incident electron of known energy E_i into the final state of energy E_f can be calculated within the one-electron theory (see Refs. 1, 6, 9, and 10 and Sec. II B). Since the incident electron can lose some portion of its energy prior to the final bremsstrahlung transition, the intensity $I(E_i)$ of XBIS radiation induced by an incident electron beam of energy E_i is[16,17]

$$I(E_i) \sim w(E_i) + \int_{E_F}^{E_i} w(E') L(E_i - E') dE' \ , \tag{3}$$

where $L(E)$ is the electron energy-loss function. If no sharp (e.g., plasmon) peaks occur in $L(E)$, the second term in (3) can be substituted by a smooth energy-dependent background. Subtracting this background from the experimental curve, the remaining oscillations are directly comparable with the calculated probability $w(E)$. This paper deals exclusively with the problem of calculating this one-electron probability $w(E)$.

B. Fundamental equations

We want to study an electron, the development of which can be described by an effective one-particle Hamiltonian H. In order to evaluate the intensity of the bremsstrahlung radiation, we must calculate the probability of a transition from the initial state $|0\rangle|\psi_i\rangle$ (describing the photon vacuum $|0\rangle$ plus the incident electron state $|\psi_i\rangle$, which must itself be an eigenstate of H) into any of the states $|\mathbf{q}\lambda\rangle|\psi_\nu\rangle$ (where $|\mathbf{q}\lambda\rangle$ describes the presence of one photon with an impulse $\mathbf{q}$ and a polarization λ, and $|\psi_\nu\rangle$ is any vector of some complete set of eigenvectors of H). This probability is according to the golden rule

$$w = \frac{2\pi}{\hbar} \sum_\lambda \int d\nu |\langle 0|\langle \psi_i|H_I|\psi_\nu\rangle|\mathbf{q}\lambda\rangle|^2 \delta(E_i - \hbar\omega - E_\nu) \ , \tag{4}$$

where H_I is the Hamiltonian of the radiative electromagnetic interaction. Since the polarization of the bremsstrahlung radiation is usually not measured, both independent polarizations must be added in order to obtain unpolarized spectra. Equation (4) can be rewritten into

$$w = \frac{2\pi}{\hbar} \sum_\lambda \int d\nu |\langle \psi_i|K_\lambda|\psi_\nu\rangle|^2 \delta(E_i - \hbar\omega - E_\nu) \ , \tag{5}$$

where

$$K_\lambda = C \frac{1}{\sqrt{\hbar\omega}} \frac{e}{m} \exp\left[-\frac{i}{\hbar}\mathbf{q}\cdot\mathbf{X}\right] \epsilon_\lambda \cdot \mathbf{P} \ . \tag{6}$$

ϵ_λ is the polarization vector, $\mathbf{q}$ is the impulse of the emitted photon ($cq = \hbar\omega$), $\mathbf{P}$ is the impulse operator of an electron, and the constant C depends upon units and normalization conditions.

We assume that the potential inside the solid has a muffin-tin form. The solution $|\psi_i\rangle$ of the Lippman-Schwinger equation

$$|\psi_i\rangle = |\mathbf{p}\rangle + G_0(E_i) V^0 |\psi_i\rangle \ , \tag{7}$$

where $G_0(E_i)$ stands for the free-electron Green function

$$G_0(E) = \frac{1}{E - H_0 + i\varepsilon} \tag{8}$$

(the operator H_0 is a free-electron Hamiltonian $H_0 = P^2/2m$), is taken for the initial electron state. Since we do not consider interaction of the incident electron with any other atom than the central one,[1,9] the potential V^0 is equal to the spherically symmetric part of the muffin-tin potential inside the central muffin-tin sphere and is zero everywhere else. Therefore, the wave function $\psi_i(\mathbf{r})$ has the form[18]

$$\psi_i(\mathbf{r}) = \sum_{l'} \frac{(2l'+1)}{4\pi\hbar^{3/2}} \frac{1}{k'} \exp[i\delta^0_{l'}(k')] R^0_{k'l'}(r) P_{l'}(\mathbf{k}'\cdot\mathbf{r}) \ , \tag{9}$$

where k' is the wave number of the incident electron ($E_i = \hbar^2 k'^2/2m$), $P_{l'}$ is the Legendre polynomial, and $R^0_{k'l'}$ is a solution of the radial Schrödinger equation in the presence of potential V^0, matching on to

$$\sqrt{2/\pi} k [j_{l'}(k'r)\cos\delta^0_{l'} - n_{l'}(k'r)\sin\delta^0_{l'}] \ , \tag{10}$$

which is its exact solution in the constant potential region outside the muffin-tin sphere.

It is convenient to introduce the Green function $G(E)$ of the final-state electron into Eq. (5), obtaining (cf. Ref. 19 for an analogous formula in the case of XAS)

$$w = -\frac{2}{\hbar} \mathrm{Im} \sum_\lambda \langle \psi_i|K_\lambda^+ G(E_i - \hbar\omega) K_\lambda|\psi_i\rangle \ , \tag{11}$$

where the Green function is defined as

$$G(E) = \frac{1}{E - H + i\varepsilon} \ . \tag{12}$$

Covering the whole infinite crystal by nonoverlapping cells of arbitrary shape, each of them containing one atom ("scattering center"), we can write (11) in the form (see Fig. 1)

$$w = -\frac{2}{\hbar} \mathrm{Im} \sum_\lambda \sum_{p,s} \int_p d^3r \int_s d^3r' \langle \psi_i|K_\lambda^+|\mathbf{r} + \mathbf{R}^p\rangle \times G(\mathbf{r} + \mathbf{R}^p, \mathbf{r}' + \mathbf{R}^s) \times \langle \mathbf{r}' + \mathbf{R}^s|K_\lambda|\psi_i\rangle \ , \tag{13}$$

where the sum $\sum_p$ runs over each of the nonoverlapping cells and the symbol $\int_p d^3r$ denotes integration over the cell, the center of which is $\mathbf{R}^p$. We also decompose the effective one-electron potential H

$$H(\mathbf{r}) = -\frac{\hbar^2}{2m}\nabla^2 + \sum_p V^p(\mathbf{r}) \ , \tag{14}$$

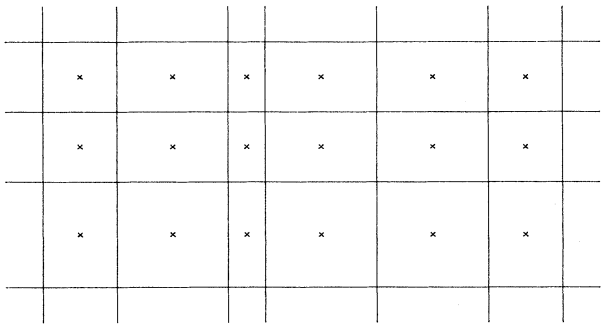

FIG. 1. An example of a coverage of the solid by a set of nonoverlapping cells, each containing one scattering center.

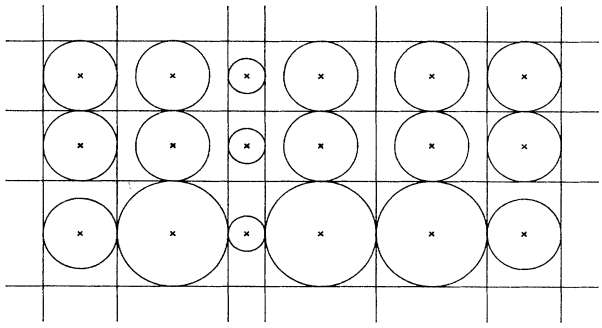

FIG. 2. An example of a coverage of the solid by a set of nonoverlapping cells with inscribed muffin-tin spheres.

where $V^p(\mathbf{r})$ is equal to the spherically symmetric part of the muffin-tin potential inside the sphere around $\mathbf{R}^p$ and is zero outside this sphere. The index 0 refers to the central atom of the cluster in the whole paper. For $p=0$, the potential of the central atom is obtained. The basic idea of the FC-MS approach is to insert the "multiple-scattering expansion" of the Green function $G(\mathbf{r}+\mathbf{R}^p,\mathbf{r}'+\mathbf{R}^s)$ into Eq. (13). For $\mathbf{r},\mathbf{r}'$ inside "muffin-tin spheres" (see Fig. 2), we can write this expansion in the form[20] (the symbol L is a multiindex, $L=\{lm\}$)

$$G(\mathbf{r}+\mathbf{R}^m,\mathbf{r}'+\mathbf{R}^n)=G_s^m(\mathbf{r},\mathbf{r}')\delta_{mn}+\sum_{L,L'}\frac{2m}{\hbar^2}\tilde{Q}_L^m(\mathbf{r})\tilde{G}_{LL'}^{mn}\tilde{Q}_{L'}^n(\mathbf{r}') , \quad (15)$$

where $G_s^m(\mathbf{r},\mathbf{r}')$ satisfies

$$G_s^m(\mathbf{r},\mathbf{r}')=G_0(\mathbf{r},\mathbf{r}')+\int d^3r''G_0(\mathbf{r},\mathbf{r}'')V^m(\mathbf{r}'')G_s^m(\mathbf{r}'',\mathbf{r}') . \quad (16)$$

The function $\tilde{Q}_L^m(\mathbf{r})$ is determined by the equation

$$\tilde{Q}_L^m(\mathbf{r})=j_l(kr)\tilde{Y}(\mathbf{r})+\int d^3r''G_0(\mathbf{r},\mathbf{r}'')V^m(\mathbf{r}'')\tilde{Q}_L^m(\mathbf{r}'') \quad (17)$$

[$\tilde{Y}_L(\mathbf{r})$ is a real spherical harmonic], and $\tilde{G}_{LL'}^{mn}$ satisfies

$$\tilde{G}_{LL'}^{mn}=\tilde{g}_{LL'}^{mn}+\sum_{L'',L'''}\sum_p\frac{2m}{\hbar^2}\tilde{g}_{LL''}^{mp}\frac{\pi}{2k^2}\tilde{t}_{L''L'''}^{p}\tilde{G}_{L'''L'}^{pn} . \quad (18)$$

The transition-matrix element $\tilde{t}_{L''}^{p}$ is defined as

$$\tilde{t}_{L''}^{p}=\frac{2k^2}{\pi}\int d^3r\, j_l(kr)\tilde{Y}_L(\mathbf{r})V^p(\mathbf{r})\tilde{Q}_{L'}^{p}(\mathbf{r}) \quad (19)$$

and

$$\tilde{g}_{LL'}^{mn}=-4\pi(1-\delta_{mn})ik\times\sum_{L''}i^{l+l''-l'}h_{l''}^{(+)}(k|\mathbf{R}^m-\mathbf{R}^n|)\tilde{Y}_{L''}(\mathbf{R}^m-\mathbf{R}^n)\times\tilde{C}_{LL'L''} , \quad (20)$$

where the Gaunt numbers are defined as

$$\tilde{C}_{LL'L''}=\int d^2n\,\tilde{Y}_L(\mathbf{n})\tilde{Y}_{L'}(\mathbf{n})\tilde{Y}_{L''}(\mathbf{n}) . \quad (21)$$

There has been a vivid controversy about the conditions which must be satisfied for the expansion (15) to be valid.[20,21] Although the results of many authors seem to indicate that the condition of confinement of $\mathbf{r},\mathbf{r}'$ inside the muffin-tin spheres can be abandoned, this is not a generally accepted opinion. In order not to interfere with this discussion, we circumvent the whole problem by introducing additional nonoverlapping "empty" spheres (Fig. 3): Taking the number of these spheres sufficiently high, we can reduce the volume of the remaining nonspherical part of the original cell below any arbitrarily small value. Thus, using the expansion of the Green function $G(\mathbf{r}+\mathbf{R}^p,\mathbf{r}'+\mathbf{R}^s)$ inside each of such spheres, we can write (with an arbitrary accuracy)

$$w=-\frac{2}{\hbar}\mathrm{Im}\sum_\lambda\sum_{p,s}\int_{\mathrm{sph}(p)}d^3r\int_{\mathrm{sph}(s)}d^3r'\langle\psi_i|K_\lambda^+|\mathbf{r}+\mathbf{R}^p\rangle G(\mathbf{r}+\mathbf{R}^p,\mathbf{r}'+\mathbf{R}^s)\langle\mathbf{r}'+\mathbf{R}^s|K_\lambda|\psi_i\rangle , \quad (22)$$

where $\sum_a$ sums over all inscribed nonoverlapping spheres and $\int_{\mathrm{sph}(a)}$ denotes integration inside such an inscribed sphere with center $\mathbf{R}^a$.

The next step consists in creating an approximate version of Eq. (15), replacing

$$\delta_{ab}G_s^a(\mathbf{r},\mathbf{r}')\rightarrow\delta_{ab}G_s^0(\mathbf{r},\mathbf{r}') , \quad (23)$$

$$\tilde{Q}_L^a(\mathbf{r})\tilde{G}_{LL'}^{ab}\tilde{Q}_{L'}^b(\mathbf{r}')\rightarrow\tilde{Q}_{L'}^0(\mathbf{r})\tilde{G}_{LL'}^{00}\tilde{Q}_{L'}^0(\mathbf{r}') . \quad (24)$$

The physical interpretation of the substitution (23) and (24) is that we neglect the deceleration of the incident electron in the field of all atoms but the central one. This is a reasonable assumption: the initial-state electron must lose a great portion of its energy in the XBIS process and hence it is highly improbable that such a loss could be

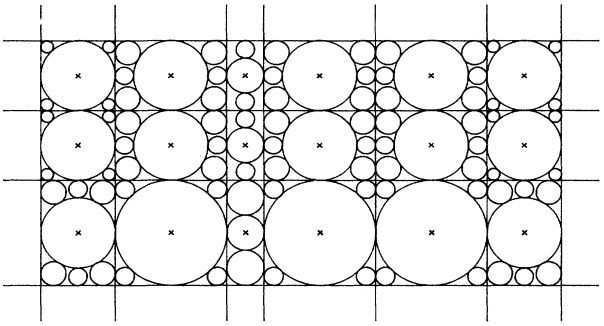

FIG. 3. An example of inscribing additional empty spheres into nonspherical cells (see also Figs. 1 and 2).

caused due to interaction with distant atoms. A more quantitative argument in favor of this so-called "single-site approximation" can be found in Ref. 22.

Inserting (23) and (24) into (22), the final expression for the XBIS transition probability can be obtained in a tedious but straightforward manner,

$$w=-\frac{2\pi^2 m^2}{\hbar^5 k^2}\mathrm{Im}\sum_{\lambda}\sum_{L,L'}(\mu_L^{\lambda})^*\frac{\tau_{LL'}^{00}}{\sin\delta_l^0\sin\delta_{l'}^0}\mu_{L'}^{\lambda} . \tag{25}$$

The matrix $\tau_{LL'}^{00}$ is determined by the equation

$$\tau_{LL'}^{ij}=t_l^i\delta_{ij}\delta_{LL'}+\sum_k\sum_{L''}t_l^i G_{LL''}^{ik}\tau_{L''L'}^{kj} , \tag{26}$$

where

$$t_l^i=-\frac{\hbar^2 k}{\pi m}\sin\delta_l^i\exp[i\delta_l^i(k)] , \tag{27}$$

$$G_{LL'}^{ij}=-(1-\delta_{mn})\frac{4i\pi^2 m}{\hbar^2 k}\times\sum_{L''}i^{l+l''-l'}h_{l''}^{(+)}(k|\mathbf{R}^m-\mathbf{R}^n|)Y_{L''}(\mathbf{R}^m-\mathbf{R}^n)\times\int d^2n\ Y_L^*(\mathbf{n})Y_{L'}(\mathbf{n})Y_{L''}^*(\mathbf{n}) \tag{28}$$

[$Y_{lm}(\mathbf{r})$ is a usual complex spherical harmonic] and

$$\mu_L=\int d^3r\ R_{kl}^0(r)Y_{lm}^*(\mathbf{r})K_\lambda\psi_i(\mathbf{r}) . \tag{29}$$

The initial wave function $\psi_i(\mathbf{r})$ is determined by Eq. (9). Having defined

$$\chi_{l'}=d_{l'}(k')R_{k'l'}^0(r)P_{l'}(\mathbf{k}'\cdot\mathbf{r}) , \tag{30}$$

$$d_{l'}(k')=\frac{(2l'+1)}{4\pi\hbar^{3/2}}i^{l'}\frac{1}{k'}\exp[i\delta_{l'}(k')] , \tag{31}$$

we can write

$$\mu_L(k)=\sum_{l'}m_{L,l'} , \tag{32}$$

$$m_{L,l'}=\int d^3r\ R_{kl}^0(r)Y_{L'}^*(\mathbf{r})K_\lambda\chi_{l'}(\mathbf{r}) . \tag{33}$$

Equations (25)–(29) can be directly used for the calculation of XBIS spectra. The crucial equation is Eq. (26). The band-structure methods profit by the use of the full translation symmetry of the problem, transforming Eq. (26) into the reciprocal, $\mathbf{k}$ space and solving the Fourier-transformed equation.[20,23] The FC-MS approach does not rely on the translation invariance and cuts off the infinite sum over lattice points $\mathbf{R}^p$ to some finite number of terms. Further analysis of Eq. (26) can be found in Sec. IV.

III. THE MATRIX-ELEMENT PROBLEM

The matrix element $m_{L,l'}$ defined by Eq. (33) poses two nontrivial problems: (i) There is a question whether the dipole approximation can be used in this case and (ii) there is a problem of numerical evaluation of the matrix element $m_{L,l'}$, since the region of integration in (33) is infinite.

It has been already suggested that the dipole approximation should be valid in XBIS since the large energy difference E_i-E_f implies the localization of the bremsstrahlung transition region. Particularly, it can be argued that the most important contribution to XBIS matrix elements comes from the region within the distance less than[16,24]

$$\rho=\frac{\hbar}{|\mathbf{p}_i-\mathbf{p}_f|} \tag{34}$$

from the atomic center ($\mathbf{p}_i$ and $\mathbf{p}_f$ are, respectively, the impulses of the initial- and final-state electrons). This distance (typically 0.01–0.1 Å) is much smaller than the wavelength of the x-ray isochromats (being 8.3 Å for the 1487-eV isochromat and 2.3 Å for the 5415-eV isochromat). Hence, the validity of the dipole approximation is generally presumed.

This presumption immediately makes it possible to bypass the problem related to the infinite boundaries of the integral (33): Neglecting the exponential factor in (6), we can express the matrix element $m_{L,l'}$ as

$$m_{L,l'}=f\int d^3r\ R_{kl}^0(r)Y_L^*(\mathbf{r})\epsilon_\lambda\cdot\mathbf{P}\chi_{l'}(\mathbf{r}) \tag{35}$$

which can be rewritten to obtain (see, e.g., Ref. 24)

$$m_{L,l'}=-\frac{i}{\omega}f\int d^3r\ R_{kl}^0(r)Y_L^*(\mathbf{r})\epsilon_\lambda\cdot\frac{dV^0}{d\mathbf{r}}\chi_{l'}(\mathbf{r}) \tag{36}$$

or

$$m_{L,l'}=-i\omega f\int d^3r\ R_{kl}^0(r)Y_L^*(\mathbf{r})\epsilon_\lambda\cdot\mathbf{r}\chi_{l'}(\mathbf{r}) , \tag{37}$$

where

$$f=C\frac{1}{\sqrt{\hbar\omega}}\frac{e}{m} \tag{38}$$

and

$$\omega=\frac{E_i-E_f}{\hbar} . \tag{39}$$

The meaning of the symbols is explained in the text following Eq. (6). The first choice (36) has an advantage of avoiding numerical problems connected with the integration: Since the potential $V^0(\mathbf{r})$ is of finite range, its gra-

dient is zero outside the muffin-tin sphere and hence the region of integration of this expression is finite.

However, there is still lack of a rigorous proof of the localization of the bremsstrahlung transition region with respect to the wavelength of emitted radiation, which is crucial for the validity of the dipole approximation. In order to make sure that the dipole approximation is really valid, it is necessary to calculate the higher multipole terms.

We concentrate on the dipole and the quadrupole electrical terms (the dipole magnetic term must be zero in a spherically symmetric potential). After substituting for $\chi_{l'}(\mathbf{r})$ from (30) to (33), the following expression for $m_{L,l'}$ can be obtained:

$$m_{L,l'} = -im\omega d_{l'}(k') \left[\int r^2 dr\, R^0_{kl}(r) r R^0_{k'l'}(r) \right] \left[\int d^2n\, Y^*_L(\mathbf{n})(\epsilon_\lambda \cdot \mathbf{n}) P_{l'}(\mathbf{k}' \cdot \mathbf{n}) \right] - \frac{m}{2c}\omega^2 d_{l'}(k') \left[\int r^2\, dr\, R^0_{kl}(r) r^2 R^0_{k'l'}(r) \right] \left[\int d^2n\, Y^*_L(\mathbf{n})(\mathbf{q} \cdot \mathbf{n})(\epsilon_\lambda \cdot \mathbf{n}) P_{l'}(\mathbf{k}' \cdot \mathbf{n}) \right] \quad (40)$$

(we denote $\mathbf{r} = r\mathbf{n}$). The first term corresponds to the dipole transition, the second one to the quadrupole transition. The integration over an infinite region can be avoided in the dipole term, choosing (36) instead of (35). However, the infinite region in the quadrupole term remains.

In order to perform integrations in (37) and (40), respectively, a special integration method must be used. The details of the procedure we used are described elsewhere;[25] its principle consists in performing the integration numerically to some $R_0 \geq R_{\mathrm{MT}}$ (R_{MT} is the muffin-tin radius) and analytically in the outer region.[26] The main advantage of this procedure is its universal applicability to any multipole terms.

In order to test the importance of the quadrupole electrical term in (40), we have calculated the atomiclike XBIS spectra of Cu [i.e., taking $t^0_l \delta_{LL'}$ instead of $\tau^{00}_{LL'}$ in Eq. (25)] using the matrix elements (40) for various isochromat energies. Analyzing theoretical XBIS spectra of atoms instead of solids is a well-founded procedure for this purpose, because the matrix element $m_{L,l'}$ is an atomiclike quantity[2] (cf. a similar analysis of electron energy-loss spectroscopy matrix elements in Ref. 27). We found that the quadrupole contribution to this spectra is negligible for both 1487 and 5415-eV isochromats: The relative changes of the bremsstrahlung radiation intensity caused by the inclusion of the quadrupole terms are smaller than 0.2% for the 1487-eV isochromat and less than 0.5% for the 5415-eV isochromat. As a result of this, the XBIS spectra calculated using matrix elements (40) agree within the thickness of the line with the spectra calculated using elements (37).

The negligibility of quadrupole terms confirms retrospectively the assumption that the radius of the bremsstrahlung transition region is smaller in order than the wavelength of x-ray isochromats (which is typically $\sim 2-8$ Å). In other words, this indicates that the decelerated electron of energy E_f comes from the core region, which is a necessary condition for Eq. (25) to be valid.

Another estimate of the spatial extension of the bremsstrahlung transition region can be made, examining the development of the "gradient" matrix element (36) with the extension of the integration region. It was demonstrated that the matrix element reaches its definitive value inside of the sphere of $R_D \approx R_{\mathrm{MT}}/4$ around the origin with a great accuracy.[1] However, this result cannot be accepted as an exact proof of the localization of the transition region, since it was obtained within the framework of the dipole approximation, which already anticipates this localization.

We calculated also the atomiclike "XBIS" spectrum for isochromat energy 10 eV. This is the energy of photons which are registered in ultraviolet BIS (inverse photoemission). Regarding that the bremsstrahlung transition region is now expected to be significantly larger than in the case of x-ray BIS, the doubts about the validity of the dipole approximation could arise. The calculation of uv BIS by means of our method has no direct physical meaning, because multiple scattering of the incident electron would also have to be taken into account for a realistic calculation at these isochromat energies. Nevertheless, it may serve as a quantitative test for the adequacy of the dipole approximation, which is commonly used in uv inverse photoemission. Our calculation of the Cu spectrum showed that for such small isochromat energies the quadrupole term really can be neglected, too—the relative changes of the bremsstrahlung intensity caused by the inclusion of quadrupole terms are smaller than 0.02%. This means nothing else than the fact that the radius of the effective bremsstrahlung transition region increases more slowly than the wavelength of the emitted radiation.

IV. MULTIPLE-SCATTERING TECHNIQUE

The size of the matrices entering Eq. (25) is formally infinite. In order to be able to use the FC-MS approach, we must cut off their dimensions at some finite value.

The physical interpretation of these equations suggest that they describe all multiple-scattering events between all atoms present in the crystal. Since various many-particle processes limit the lifetime of the scattered electron, the effective length of the scattering path is also finite. Hence, in most cases it must be sufficient to limit our investigation to some finite cluster of atoms surrounding the central one. This cuts off the sum $\sum_p$ over lattice points.

Also the double sum $\sum_{L,L'}$ can be cut off at some finite value $l = l_{\max}$, since the semiclassical trajectory would be outside the region of a nonconstant potential around the scattering center for higher l numbers and hence the probability of a scattering event would be very small.

Thus limiting the dimensions of all matrices entering Eq. (25), this equation can be solved by matrix inversion.

Solving Eq. (25) by iteration and retaining only a few terms in the series

$$\tau^{ij}_{LL'}=t^i_l\delta^{ij}_{LL'}+t^i_l G^{ij}_{LL'}t^j_{l'}(1-\delta_{LL'})(1-\delta^{ij}) + \sum_k\sum_{L''} t^i_l G^{ik}_{LL''}t^k_{l''}G^{kj}_{L''L'}t^j_{l'}+\cdots , \quad (41)$$

various approximations to the full multiple scattering can be introduced.[28,23]

Inversion of large matrices is a computationally difficult task. In order to speed up the calculation, it is very convenient to divide the whole cluster into several concentric shells and to calculate the intrashell and the intershell scattering events separately. Using the expansions[29]

$$G^{ij}_{LL'}=\begin{cases}\sum_k\sum_{L''} D^{ik}_{LL''}G^{kj}_{L''L'}, & |\mathbf{R}^i|<|\mathbf{R}^j| \quad (42)\\ \sum_k\sum_{L''} G^{ik}_{LL''}D^{kj}_{L''L'}, & |\mathbf{R}^i|>|\mathbf{R}^j| , \quad (43)\end{cases}$$

$$D^{ij}_{LL'}=\sum_{L''}4\pi i^{l-l'+l''}j_{l''}(k|\mathbf{R}^i-\mathbf{R}^j|)Y_{L''}(\mathbf{R}^i-\mathbf{R}^j) \times\int d^2n\, Y_L(\mathbf{n})Y^*_{L'}(\mathbf{n})Y_{L''}(\mathbf{n}) , \quad (44)$$

we obtain a set of equations which enable us to assemble the $\tau^{00}_{LL'}$ matrix of the whole cluster from several particular $\tau^{ij}_{LL'}$ matrices of different shells.[19]

Since the number of atoms contained in a single shell is considerably smaller than the number of atoms in the whole cluster, the size of matrices which have to be inverted due to Eq. (26) is now also smaller and a significant part of CPU time can be thus saved.

Moreover, the separate calculation of intrashell and intershell multiple scattering enables us to use different approximations to multiple scattering for different types of scattering.[28] Thus, the ratio between the accuracy of the calculation and the necessary computational effort can be optimized.

The concept of using Eqs. (42) and (43) for exploiting the division of the cluster into shells poses a new problem: another formally infinite sum over L'' occurs in the expansion (42) and (43). Since this sum must be cut off at some finite value $l''=l_{\text{out}}$, another convergence problem arises. To our knowledge, there does not exist any general method how to make an estimate of l_{out} (contrary to the "centrifugal barrier prescription" for the case of $l_{\max}$ in Eq. (25)–see, e.g., Ref. 30). We took $l_{\text{out}}=12$ in our calculations; the convergence in l_{out} is tested in Appendix A.

V. RESULTS AND DISCUSSION

In order to test the ability of the FC-MS approach to describe XBIS spectra, a comparison of computed spectra with experimental oscillations is presented in this section. We analyzed XBIS spectra of Cu and Pd for isochromat energies 1487 and 5415 eV, because the experiment for a large energy extent is available for both elements. Since the theoretical FC-MS curves presented in this paper show only the transition probability calculated from (25) and not the full XBIS intensity [which is to be calculated according to Eq. (3)], a smooth background was subtracted from the raw experiment to get the experimental oscillations (this procedure was already done in Ref. 31). If the corresponding electron energy-loss spectra do not exhibit sharp peaks, these experimental XBIS oscillations should be directly comparable to the transition probability (25).

A cluster of 79 atoms divided into five concentric shells (identical with the coordination spheres of a crystal) was taken into account in all the calculations presented here. The maximum $l_{\max}$ (see Sec. IV) varied from 3 to 6 with respect to the final-state energy E_f (greater E_f generally requires higher $l_{\max}$). We took $l_{\max}=3$ for $E_f<36$ eV, $l_{\max}=4$ for $E_f<56$ eV, $l_{\max}=5$ for $E_f<142$ eV, and $l_{\max}=6$ for higher final electron energies in the case of Cu spectra and $l_{\max}=3$ for $E_f<33$ eV, $l_{\max}=4$ for $E_f<63$ eV, and $l_{\max}=5$ for higher final electron energies in the case of Pd spectra. These energy ranges were chosen on account of the energy dependence of the magnitudes of scattering amplitudes $t_l(k)$. The convergence in $l_{\max}$ was tested in those energy regions, where the values of $l_{\max}$ changed.

The theoretical FC-MS approach curves presented in this paper were calculated according to formulas (25)–(29) for a single-crystal sample and for the angle α between the incident electron-beam direction and the registered bremsstrahlung radiation direction of $\alpha=90°$. Since both Cu and Pd are cubic symmetrical materials, the electron structure-related quantities (e.g., the scattering matrix $\tau^{00}_{LL'}$) are practically the same for both a single crystal and a polycrystal sample. As a result, the XBIS spectra are very similar for both types of a sample and we can thus compare our single-crystal results with experiments made on polycrystals (see Appendix B for a quantitative analysis). Nor is the value of the angle α crucial—the varying of α over a broad energy interval causes a mere decrease or increase of overall XBIS intensity and does not change the shape of XBIS spectra. This is demonstrated in Appendix C.

We decided not to perform any corrections of our theoretical spectra due to the lifetime broadening in order to display the theoretical results undisturbed by any optional parameter. Nevertheless, it is obvious that a suitable smearing procedure would improve the visual agreement of our theory with experiment.

We can distinguish two main sources of discrepancy between theory and experiment. First, the discrepancy may be a consequence of using an inaccurate potential. Such an effect can arise also within the band-structure approach. We discuss the choice of the potential in Secs. V A–V C. The second source of discrepancies is the restriction of our calculation to a finite part of the crystal. This restriction is inherent in the FC-MS approach and thereby cannot be avoided.

From this point of view, the agreement between the FC-MS theory and the experiment can be regarded as a test, whether the cluster is large enough. Calculations of Cu XANES suggest (see, e.g., Ref. 32) that the inclusion

of 79 atoms should be sufficient. We did not perform an entire analysis of the influence of the cluster size on XBIS spectra because of the large CPU time it would require. However, the inner resemblance between XBIS and XAS processes indicates that such an analysis should provide similar results as an analogous analysis of XAS spectra.[33]

A. Self-consistent potential—comparison with band-structure approach calculation

In order to separate these two sources of errors, we calculated at first XBIS spectra using a self-consistent electron potential taken from Ref. 34. This choice enables us a comparison of our calculations with the band-structure results,[10] where the same potential is used. These spectra are presented in Figs. 4 and 5. Identical energy scales were chosen for both isochromats in order that the changes caused by the use of different isochromat energies could be displayed. We see immediately that the FC-MS approach describes all significant features of XBIS spectra fairly well for all energies for which the experiment is available. The greatest difference between the FC-MS spectrum and both the experiment- and the band-structure-based results is in the close-to-edge region ($E_f < 10$ eV above E_F). Since the band-structure approach describes XBIS correctly in this energy region,[10,1] we assume that a larger cluster should be used in order to properly calculate XBIS also for small energies.

Apart from the full multiple-scattering calculation, a single-scattering approximation [analogous to curved-wave EXAFS (Ref. 35)] was also tested (dashed curves in Figs. 4 and 5). Although this calculation demands roughly two orders less CPU time than the full multiple-scattering calculation, the resulting spectrum still exhibits a considerable resemblance to the original full multiple-scattering curve. This is in agreement with analogous XANES calculations—it was demonstrated that a single-scattering calculation can describe XAS spectrum of Cu even in the near energy region fairly well.[35,36]

B. Comparison of a self-consistent and a non-self-consistent potential

All theoretical curves presented so far were calculated for the same self-consistent potential, which was obtained after a self-consistent band-structure calculation.[34] In order to check the possibility to investigate, e.g., amorphous materials, it is necessary to verify that the knowledge of a self-consistent potential is not crucial for

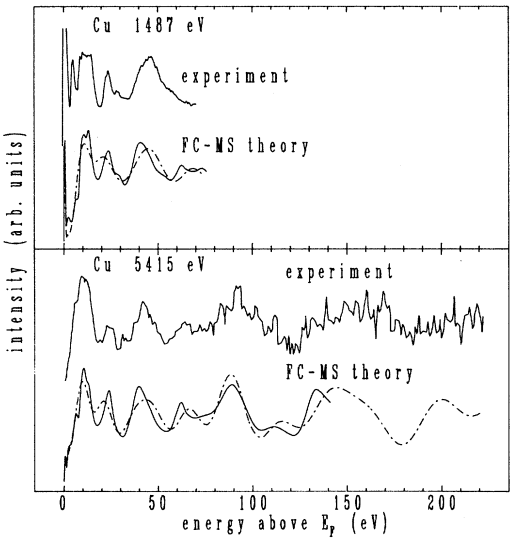

FIG. 4. Experimental XBIS oscillations of Cu for two isochromat energies compared with theoretical results. The experiment is taken from Ref. 5 (1487 eV) and from Ref. 31 (5415 eV). The solid FC-MS theoretical curves represent a full multiple-scattering calculation; the dotted-dashed FC-MS theoretical curves represent a single-scattering calculation. The self-consistent potential was used for calculation of the theoretical curves.

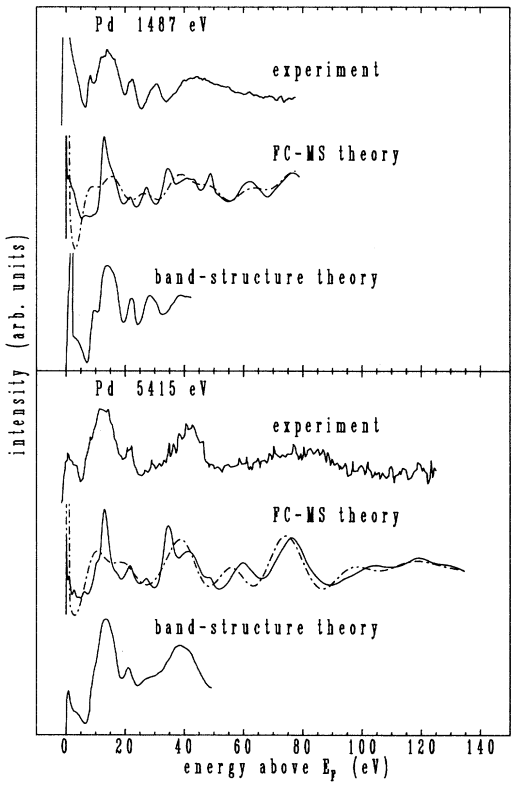

FIG. 5. Experimental XBIS oscillations of Pd for two isochromat energies compared with theoretical results. The experiment is taken from Ref. 5 (1487 eV) and from Ref. 31 (5415 eV). The solid FC-MS theoretical curves represent a full multiple-scattering calculation; the dotted-dashed FC-MS theoretical curves represent a single-scattering calculation. The lower theoretical curves calculated by a band-structure approach were taken from Ref. 10. The same self-consistent potential was used for calculation of all of the theoretical curves presented here.

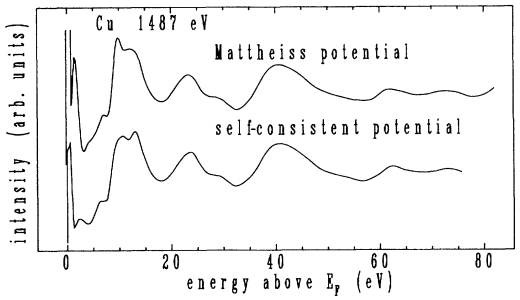

FIG. 6. Theoretical XBIS spectra of Cu (isochromat energy 1487 eV) calculated for a self-consistent potential taken from Ref. 34 and for a non-self-consistent potential constructed according to the Mattheiss prescription.

the calculation of XBIS spectra.[37]

We decided to calculate a XBIS spectrum for the so-called Mattheiss potential, since this type of potential is widely used in EXAFS and XANES studies and was shown to provide satisfactory results.[37–39] This potential is constructed via superposition of charge densities of neutral atoms located in the lattice points.[12,13] The exchange effects are treated in the same manner as in Ref. 34, i.e., approximately by using the Kohn-Sham exchange potential[14]

$$V_{\rm ex}(\mathbf{r})=-3\alpha\frac{e^2}{4\pi\varepsilon_0}\left[\frac{3n(\mathbf{r})}{8\pi}\right]^{1/3}, \tag{45}$$

where $\alpha=\frac{2}{3}$, ε_0 is the vacuum permittivity, and $n(\mathbf{r})$ is the electron density.

The results are shown in Figs. 6 and 7. Since we did not perform a band-structure calculation with the Mattheiss potential to find the Fermi level, the horizontal alignment of the corresponding spectrum was made in order to get the best accordance with the self-consistent potential spectrum. It is obvious from Figs. 6 and 7 that the results obtained for both types of potential are almost identical for final-state electron energies $E_f > 10$ eV above E_F. Thus, we can conclude that it is not necessary to use a self-consistent potential in order to get a reasonable theoretical spectrum in that energy region where the FC-MS approach is valid.

C. Energy-dependent potential

The discrepancy between the theoretically predicted and the experimentally observed positions of spectral peaks is usually attributed to the omission of the energy dependence of the effective electron potential, i.e., to the neglect of self-energy effects.[5,4] Little is known about optimal construction of such a potential and the prescriptions for it used so far do not lead to a full agreement between theory and experiment.[5] We had tested the simplest form of an energy-dependent potential, namely the Dirac-Hara exchange potential.[15] This potential is constructed so as to describe exactly the ground state of a homogeneous electron gas as calculated within the Hartree-Fock approximation and its energy-dependence is extrapolated into the excited states energy region. It has the form[40]

$$V_{\rm ex}(\mathbf{r})=-3\alpha\frac{e^2}{4\pi\epsilon_0}\left[\frac{3n(\mathbf{r})}{8\pi}\right]^{1/3}h(k)\,, \tag{46}$$

where

$$h(k)=1+\frac{1-X(k)^2}{2X(k)}\ln\left|\frac{1+X(k)}{1-X(k)}\right|\,,$$

$$X(k)=\frac{E_k}{E_0(\mathbf{r})}\,.$$

$E_0(\mathbf{r})=\hbar^2/2m[3\pi^2 n(\mathbf{r})]^{2/3}$ is "the local Fermi energy" and E_k is the final-state electron energy measured with respect to the same "zero level" as $E_0(\mathbf{r})$ (see Ref. 15 for a more detailed discussion).

Figure 8 presents the experimental Cu spectrum to-

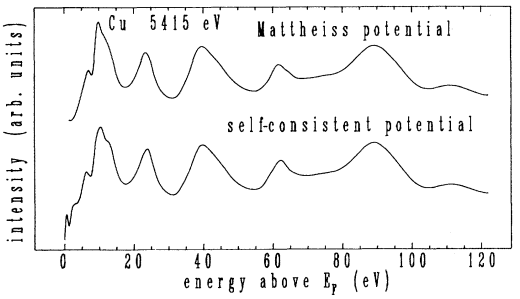

FIG. 7. Theoretical XBIS spectra of Cu (isochromat energy 5415 eV) calculated for a self-consistent potential taken from Ref. 34 and for a non-self-consistent potential constructed according to the Mattheiss prescription.

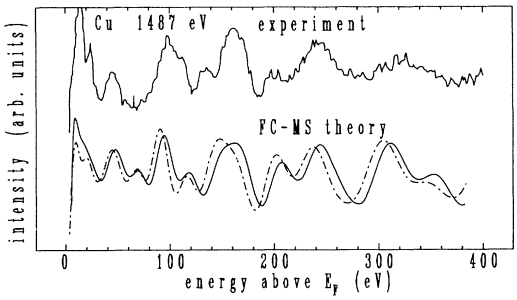

FIG. 8. Comparison of theoretical FC-MS XBIS spectra of Cu (isochromat energy 1487 eV) for a Kohn-Sham exchange term (dotted-dashed lower line) and for an energy-dependent Dirac-Hara exchange term (solid lower line). The experiment was taken from Ref. 4; the potential was constructed according to the Mattheiss prescription.

gether with the theoretical spectrum (calculated within the single-scattering approximation), obtained for the Mattheiss potential with the Kohn-Sham exchange term (45) and with the Dirac-Hara exchange term (46). Although the single-scattering approximation does not describe all details of the Cu spectrum properly in the whole energy range (cf. Fig. 4 and Ref. 36), the general features of the experimental spectrum are well reproduced. Evidently, using the Dirac-Hara exchange term shifts the positions of main peaks to higher energies. This shift is nearly 10 eV in the extended part of the spectrum. It removes much of the discrepancy between the experiment and the theoretical spectrum based on the Kohn-Sham exchange term (45), in accordance with similar XAS studies.[41–43] However, because of the above-mentioned uncertainty concerning the validity of the single-scattering approximation, a more detailed analysis based on a multiple-scattering calculation would be necessary to quantify the merit of the Dirac-Hara exchange potential properly.

VI. CONCLUSION

Like more familiar x-ray-absorption spectroscopy, XBIS provides us with information about unoccupied electron states. However, it is more difficult to extract relevant information from the XBIS spectrum than from the XAS spectrum. The XBIS spectra lack both the sharp separation of particular l components [because the initial state is a mixture of several l symmetries—cf. Eq. (9)] and the chemical selectivity of XAS (guaranteed by different energy positions of distinct absorption edges). Nevertheless, there exists a possibility for XBIS to compensate these disadvantages at least partially.

Since the relative weight of individual l components in the total XBIS spectrum depends on the isochromat energy, different views on the unoccupied electron states are obtained using a different "color" of isochromats.[44,2,10] Moreover, the magnitudes of XBIS matrix elements depend on the atomic number.[1] Therefore, we can assume that the XBIS spectrum of a material which is composed of both light and heavy atoms will reflect predominantly

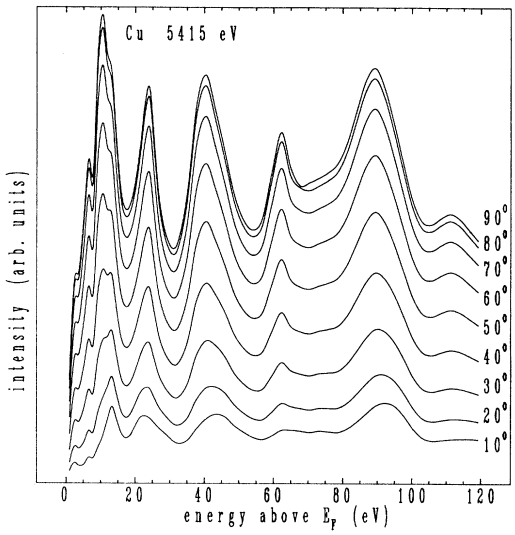

FIG. 10. FC-MS theoretical spectra of Cu (isochromat energy 5415 eV) calculated for different values of the angle α between the direction of the incident electron beam and the direction of the emitted bremsstrahlung radiation. The angle α varies from $\alpha=90°$ (the uppermost curve) to $\alpha=10°$ (the lowest curve). A self-consistent potential taken from Ref. 34 was used.

those electron states which are related to the deceleration of the incident electron on the heavy atom. Hence, both l separation and some sort of chemical selectivity can be achieved in XBIS, too.

The ability of the finite-cluster multiple-scattering theory, which does not rely on Bloch's theorem, to describe the XBIS spectra correctly increases further the possibility of extracting relevant information from these spectra. Adequacy of the FC-MS approach to the XBIS theory enables us to calculate XBIS spectra in an extended energy range, where the application of band-structure methods is extremely difficult.[45] Using the FC-MS approach is also a natural way for calculating XBIS of materials lacking full translation invariance (surfaces, amor-

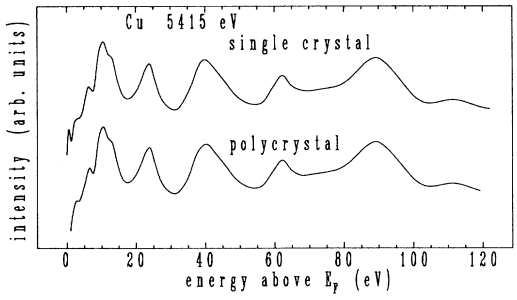

FIG. 9. FC-MS theortical XBIS spectra of Cu (isochromat energy 5415 eV) calculated for a single-crystal sample and for a polycrystal sample. A self-consistent potential taken from Ref. 34 was used.

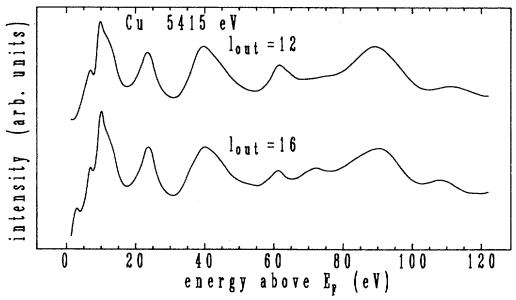

FIG. 11. FC-MS theoretical XBIS spectra of Cu (isochromat energy 5415 eV) calculated for two choices of l_{out}. The potential constructed according to the Mattheiss prescription was used.

phous materials).

Finally, application of the FC-MS formalism in XBIS and XAS calculations can help us to understand the processes underlying XAS: e.g., an interesting possibility of evaluating the role of the core-hole effect in XAS arises from calculating the XAS spectrum (including the core-hole effect) and the XBIS spectrum (where no core hole is present) by means of the same method.

APPENDIX A: CONVERGENCE IN l_{out}

The division of the cluster into several shells and subsequent assembling the total $\tau^{00}_{LL'}$ matrix from the scattering matrices of particular shells [see Eqs. (42) and (43)] introduces another formally infinite sum over L. All results presented in Figs. 4–8 (and also in Figs. 9 and 10) were calculated cutting off this sum at $l_{\text{out}}=12$. In order to test convergency in this cutting, another XBIS spectrum of Cu was calculated for $l_{\text{out}}=16$ (Mattheiss potential was used). A comparison of both spectra (for $l_{\text{out}}=12$ and for $l_{\text{out}}=16$) is displayed in Fig. 11. It demonstrates that adding more terms to the L'' sum in Eqs. (42) and (43) (i.e., increasing of l_{out}) does not affect the result significantly.

APPENDIX B: XBIS SPECTRUM FOR POLYCRYSTALS

The FC-MS spectra presented in Figs. 4–8 were calculated according to Eqs. (25)–(29), i.e., for a single-crystal sample. In order to compare these theoretical spectra with experiments on polycrystals,[5,31] the averaging of calculated spectra over all possible orientations of a single-crystal sample is necessary. Corresponding equations are similar to Eqs. (25)–(29), since only the matrix elements $\mu_L(k)$ are involved in such an averaging. We do not present them here because they are formally too complicated. They follow directly from the integration of Eq. (25) with respect to the orientation of vectors $\mathbf{q}$ and $\mathbf{k}'$, holding the angle between them fixed [see Eqs. (33), (6), and (30)].

The averaged spectrum of Cu is presented in Fig. 9 (the self-consistent potential was used here). It is very similar to the single-crystal spectrum, which is not surprising: Since the muffin-tin potential was used, the atomiclike matrix elements $m_{l,L'}$ must be invariant with respect to any rotation of the sample, and since both Cu and Pd crystals are cubic symmetrical, the electron structure must be rotationally invariant for $l\leq 1$. As the matrix elements $m_{l,L'}$ are negligible for $l\geq 3$ (Ref. 2), only the d states can introduce some rotational asymmetry. Figure 9 indicates that this effect is very small. Hence, it is reasonable to compare the experiments made on polycrystals with theoretical spectra calculated according to Eqs. (25)–(29) which are strictly valid only for single crystals.

APPENDIX C: ANGULAR DEPENDENCE OF XBIS SPECTRA

All theoretical spectra presented in Figs. 4–9 and 11 were calculated for the angle α between the incident electron-beam direction and the detected radiation direction of $\alpha=90°$. This is true for the experimental spectra of 5415-eV isochromat energy,[46] but not of 1487 eV, where this angle is near to $\approx 40°$ (Ref. 47). Figure 10 shows calculated polycrystalline-sample spectra of Cu for several angles α. The structure of these spectral curves is almost identical for $\alpha>20°$. Hence, varying the angle α causes a mere overall multiplicativelike shift of the XBIS intensity, which is not the subject of comparison between the computed and the experimental spectra.

[1] W. Speier, J. C. Fuggle, P. Durham, R. Zeller, R. J. Blake, and P. Sterne, J. Phys. C **21**, 2621 (1988).

[2] A. Šimůnek, J. Vackář, and E. Sobczak, Phys. Rev. B **38**, 8515 (1988).

[3] J. Vackář and A. Šimůnek, Physica B&C **158B**, 572 (1989).

[4] W. Speier, J. C. Fuggle, R. Zeller, and M. Campagna, in *EXAFS and Near Edge Structure III,* edited by K. O. Hodgson, B. Hedman, and J. E. Penner-Hahn (Springer, Berlin, 1984), p. 496.

[5] W. Speier, R. Zeller, and J. C. Fuggle, Phys. Rev. B **32**, 3597 (1985).

[6] J. E. Müller, in *EXAFS and Near Edge Structure III,* edited by K. O. Hodgson, B. Hedman, and J. E. Penner-Hahn (Springer, Berlin, 1984), p. 7.

[7] W. Speier, T. M. Hayes, J. W. Allen, J. B. Boyce, J. C. Fuggle, and M. Campagna, Phys. Rev. Lett. **55**, 1963 (1985).

[8] E. Sobczak and J. Auleytner, Phys. Rev. B **37**, 6251 (1988).

[9] A. Šimůnek, O. Šipr, and J. Vackář, Phys. Rev. Lett. **63**, 2076 (1989).

[10] W. Speier, J. Phys. C **21**, L1183 (1988).

[11] E. A. Stern, J. Phys. (Paris) Colloq. **47**, C8-3 (1986).

[12] L. Mattheiss, Phys. Rev. **133**, A1399 (1964).

[13] L. Mattheiss, Phys. Rev. **134**, A970 (1964).

[14] W. Kohn and L. J. Sham, Phys. Rev. **140**, A1133 (1965).

[15] S. Hara, J. Phys. Soc. Jpn. **22**, 710 (1967).

[16] P. E. Best and C. C. Chu, Phys. Rev. B **15**, 5160 (1977).

[17] H. J. W. M. Hoekstra, W. Speier, R. Zeller, and J. C. Fuggle, Phys. Rev. B **34**, 5177 (1986).

[18] See, e.g., L. I. Schiff, *Quantum Mechanics* (McGraw-Hill, New York, 1968).

[19] P. J. Durham, J. B. Pendry, and C. H. Hodges, Comput. Phys. Commun. **25**, 193 (1982).

[20] R. Zeller, J. Phys. C **20**, 2347 (1987).

[21] A. R. Williams and J. van W. Morgan, J. Phys. C **5**, L293 (1972); J. S. Faulkner, Phys. Rev. B **19**, 6186 (1979); R. G. Brown, J. Phys. B **21**, L309 (1988) and references therein.

[22] H. Winter, P. J. Durham, and G. M. Stocks, J. Phys. F **14**, 1047 (1984).

[23] C. R. Natoli and M. Benfatto, J. Phys. (Paris) Colloq. **47**, C8-11 (1986).

[24] H. A. Bethe and E. E. Salpeter, in *Handbuch der Physik,* edited by S. Flügge (Springer, Berlin, 1957), Vol. 35, p. 88.

[25] J. Vackář, A Šimůnek, and O. Šipr, Comput. Phys. Commun. **66**, 259 (1991).

[26] M. S. Pindzola and H. P. Kelly, Phys. Rev. A **14**, 204 (1976).

[27] D. K. Saldin and J. M. Yao, Phys. Rev. B **41**, 52 (1990).

[28]D. D. Vvedensky, D. K. Saldin, and J. B. Pendry, Comput. Phys. Commun. **40**, 421 (1986).
[29]P. Lloyd and P. V. Smith, Adv. Phys. **21**, 69 (1972).
[30]A. Messiah, *Quantum Mechanics* (North-Holland, Amsterdam, 1961).
[31]E. Sobczak and J. Auleytner, J. Phys. (Paris) Colloq. **48**, C9-1121 (1987).
[32]G. N. Greaves, P. J. Durham, G. Diakun, and P. Quinn, Nature **294**, 139 (1981).
[33]L. A. Bugaev, I. I. Gegusin, O. A. Novakovich, and R. V. Vedrinskii, J. Phys. (Paris) Colloq. **47**, C8-101 (1986); P. Sainctavit, J. Petiau, G. Calas, M. Benfatto, and C. R. Natoli, *ibid.* **48**, C9-1109 (1987).
[34]V. L. Moruzzi, J. F. Janak, and A. R. Williams, *Calculated Electronic Properties of Metals* (Pergamon, New York, 1978).
[35]J. E. Müller and W. L. Schaich, Phys. Rev. B **27**, 6489 (1983).
[36]J. Rehr and R. C. Albers, Phys. Rev. B **41**, 8139 (1990).
[37]D. Norman, K. B. Garg, and P. J. Durham, Solid State Commun. **56**, 895 (1985).
[38]M. Kitamura, S. Muramatsu, and C. Sugiura, Phys. Rev. B **33**, 5294 (1986).
[39]L. T. Wille, P. J. Durham, and P. A. Sterne, J. Phys. (Paris) Colloq. **47**, C8-43 (1986).
[40]N. W. Ashcroft and N. D. Mermin, *Solid State Physics* (Holt, Rinehart and Winston, New York, 1976).
[41]S.-H. Chou, J. J. Rehr, E. A. Stern, and E. R. Davidson, Phys. Rev. B **35**, 2604 (1987).
[42]S.-H. Chou, F. W. Kutzler, D. E. Ellis, G. K. Shenoy, T. J. Morrison, and P. A. Montano, Phys. Rev. B **31**, 1069 (1985).
[43]P. Sainctavit, J. Petiau, M. Benfatto, and C. R. Natoli, Physica B **158**, 347 (1989).
[44]C. C. Chu and P. E. Best, Phys. Rev. B **19**, 3414 (1979).
[45]R. C. Albers, Physica B **158**, 372 (1989).
[46]E. Sobczak (private communication).
[47]W. Speier (private communication).